Available online at www.sciencedirect.com
ScienceDirect
European Journal of Mechanics B/Fluids 27 (2008) 539–551

Absolute and convective instabilities of two-dimensional bluff body wakes in ground effect

Takafumi Nishino, Graham T. Roberts *

School of Engineering Sciences, University of Southampton, Southampton, SO17 1BJ, United Kingdom

Received 19 December 2006; received in revised form 26 May 2007; accepted 25 September 2007

Available online 18 October 2007

Abstract

Local and global instabilities are investigated of wakes of general two-dimensional bluff bodies placed near and parallel to a plane boundary or ground. A spatio-temporal linear stability analysis is first applied to a four-parameter family of local wake profiles to investigate the fundamental local stability characteristics of the wake in ground effect. The analysis shows significant dependencies of the stability characteristics of the wake on the distance from the wake centreline to the ground (normalised by the wake width), and also on the velocity ratio of the near- and far-ground sides of the wake. The analysis is then compared with earlier experiments on a circular cylinder to examine, according to the transition scenario of the steep global modes, the streamwise variation of the local stability characteristics of the wake in ground effect. The comparison indicates that the near wake region of the cylinder changes from being absolutely unstable to being convectively unstable when the cylinder comes down into the near-ground range in which the von Kármán-type vortex shedding from the cylinder is suppressed, being qualitatively consistent with the transition scenario for general wake-type flows. A possible explanation is also given for the counter-intuitive relation between the thickness of the boundary layer on the ground and the critical gap distance for the cessation of the von Kármán-type vortex shedding in ground effect.

Keywords: Absolute instability; Bluff body wake; Circular cylinder; Vortex shedding; Ground effect

1. Introduction

The onset and cessation of von Kármán-type vortex shedding from cylindrical bluff bodies are of fundamental interest as well as of great importance in fluid mechanics. This type of vortex shedding may significantly affect various fluid-mechanical properties of practical interest, such as flow-induced forces, vibrations and noise, and the efficiencies of heat and mass transfer. Recent studies show that the Kármán vortex shedding may be explained as a result of absolute instability in the near wake region, which allows local disturbances to propagate both upstream and downstream and thus produces a resonance between the travelling instability waves (see Huerre and Monkewitz [1] and Huerre [2] for comprehensive reviews). For example, a linear stability analysis by Monkewitz [3] shows the existence of an absolutely unstable region in the near wake region of a circular cylinder at the critical Reynolds

* Corresponding author. Tel.: +44 23 8059 2325; fax: +44 23 8059 3058.
E-mail address: gtr@soton.ac.uk (G.T. Roberts).

0997-7546/$ – see front matter
doi:10.1016/j.euromechflu.2007.09.006

number of about 50 for the onset of the Kármán vortex shedding. In analogy to this, the cessation of the vortex shedding at much higher Reynolds numbers behind a cylinder equipped with a backward splitter plate, which was first experimentally observed by Roshko [4], may also be explained because the splitter plate prevents the hydrodynamic resonance in the near wake region [5].

Another example of the onset/cessation of the Kármán vortex shedding — the mechanisms of which, however, are still unclear — is that observed behind a cylinder placed near and parallel to a plane boundary or ground. The focus of the present study is on this type of flow, which is encountered in many engineering applications and has been experimentally investigated by several researchers [6–9]. The onset and cessation of the Kármán vortex shedding in this flow configuration is governed not only by the Reynolds number Re but also by the gap ratio, i.e., the ratio of the gap distance between the cylinder and the ground, h, to the cylinder diameter d. For a circular cylinder in the so-called 'upper-subcritical' Reynolds number regime ($2.0 \times 10^4 < Re < 2.0 \times 10^5$), Bearman and Zdravkovich [6] reported that the vortex shedding was suppressed at $h/d < 0.3$. It should be noted that, in their study, the cylinder was partially submerged in the boundary layer of $0.8d$ thickness formed on the ground. The influence of the thickness of the boundary layer was later investigated by Lei et al. [7]; the critical gap ratio for the onset/cessation of the Kármán vortex shedding slightly decreased from 0.3 to 0.2 as the boundary layer thickness *increased* (which is counter-intuitive but is discussed further later in this paper). More recently, the present authors [9] observed that the Kármán vortex shedding was suppressed at $h/d < 0.35$ even when the cylinder was placed near a moving ground, on which substantially no boundary layer developed since the ground was running at the same speed as the freestream. These results suggest that the cessation of the Kármán vortex shedding in ground effect cannot be fully explained by the blockage of the flow through the gap between the cylinder and the ground, which should only be the case when the cylinder is very close to the ground.

The main objective of the present study is to examine another possible explanation for the cessation of the Kármán vortex shedding in ground effect, which is that the ground does not prevent the flow through the gap but does restrict the propagation of disturbances in the near wake region and hence suppresses the resulting Kármán vortex shedding, in analogy to the backward splitter plate described above. Although the near wake structures of two-dimensional bluff bodies are in general three-dimensional unless the Reynolds number of the flow is very low (e.g., $Re <$ 180–190 for a circular cylinder in a free stream [10]) and also nonlinear effects are of importance for the physics of the Kármán vortex shedding, this study employs a local (i.e., parallel-assumed) linear stability analysis to understand the fundamental, qualitative stability characteristics of the wakes in ground effect. It is also assumed that the fluid is inviscid and incompressible. The analysis is first applied to a four-parameter family of velocity profiles, which is an extended version of a two-parameter symmetric near wake model by Monkewitz and Nguyen [11] and Monkewitz [3], in order to investigate the local absolute and local convective instabilities of the wakes in ground effect. The results of the analysis are then compared with the earlier experiments by the authors [9]. Specifically, the streamwise variation of the local linear stability characteristics of the wake is examined to discuss the link between the local linear stability characteristics and the cessation of the Kármán vortex shedding in ground effect. The discussion is based on the transition scenario of 'steep global modes' by Pier and Huerre [12], in which the upstream edge of the region of local linear absolute instability acts as a wavemaker to generate nonlinear travelling waves in the downstream direction (cf. Section 4.3).

In the following, the details of the wake model and the analysis procedure will be described in Sections 2 and 3, respectively, and then the results of the analysis will be presented in Section 4. Finally a concluding summary will be given in Section 5.

2. Near wake model

The local velocity profile of the near wake of general two-dimensional bluff bodies placed near a ground may be approximated by the following analytical model equations:

$$U(y) = \left[1 - R_1 + 2R_1 F_1(y)\right](U_c + U_\infty)/2 \quad (\text{for } 0 \leqslant y \leqslant \infty), \tag{1}$$

$$U(y) = \left[1 - R_2 + 2R_2 F_2(y)\right](U_c + U_g)/2 \quad (\text{for } -H \leqslant y < 0), \tag{2}$$

where

$$R_1 = (U_c - U_\infty)/(U_c + U_\infty), \qquad F_1(y) = \left\{1 + \sinh^{2N_1}\left[y \sinh^{-1}(1)/b_1\right]\right\}^{-1}, \tag{3}$$

$$R_2 = (U_c - U_g)/(U_c + U_g), \qquad F_2(y) = \left\{1 + \sinh^{2N_2}\left[y \sinh^{-1}(1)/b_2\right]\right\}^{-1}, \tag{4}$$

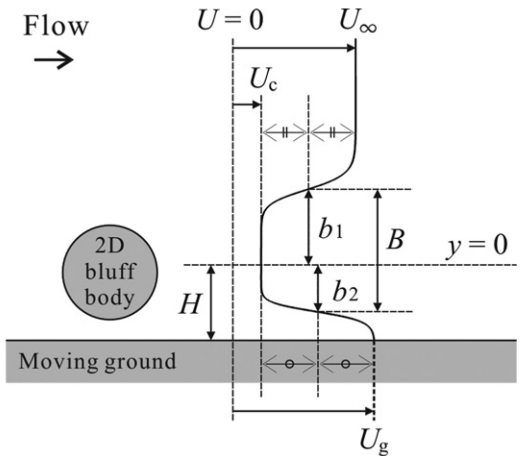

Fig. 1. Near wake model of general two-dimensional bluff bodies in ground effect (note that $b_1 = b_2 = B/2$ in the present study).

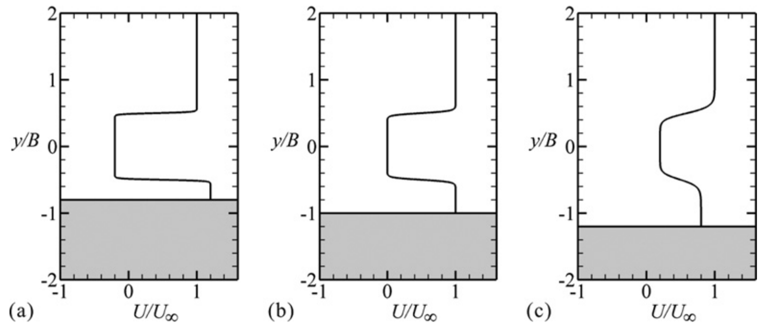

Fig. 2. Examples of local wake profiles in ground effect. (a) $N = 25$, $U_g/U_\infty = 1.2$, $U_c/U_\infty = -0.2$, $H/B = 0.8$; (b) $N = 12.5$, $U_g/U_\infty = 1$, $U_c/U_\infty = 0$, $H/B = 1$; (c) $N = 4$, $U_g/U_\infty = 0.8$, $U_c/U_\infty = 0.2$, $H/B = 1.2$.

as described in Fig. 1. Here U_c and U_∞ indicate the velocities at $y = 0$ and ∞, respectively. U_g is a hypothetical velocity at $y = -\infty$, and H is the transverse distance between $y = 0$ and the ground. N_1 and N_2 determine the ratio of each mixing layer thickness to the width of the wake, and b_1 and b_2 are the so-called 'half-widths' of the wake, which are respectively the distances from $y = 0$ to the points where $U(y) = (U_c + U_\infty)/2$ for b_1 and $U(y) = (U_c + U_g)/2$ for b_2. It should be noted that this model is an extended asymmetric version of the symmetric near wake model by Monkewitz and Nguyen [11] and Monkewitz [3], which can be reproduced from the above equations with $U_g = U_\infty$, $N_1 = N_2$, $b_1 = b_2$, and $H = \infty$.

Since the primary objective is to examine the fundamental influence of the nearby ground on the stability characteristics of the wake, $N_1 = N_2 = N$ and $b_1 = b_2 = B/2$ are also employed in this study for simplicity. It follows that U_∞ and B are the characteristic velocity and length of the flow (but note that B varies in the streamwise direction when the global instability of the wake is discussed later in Section 4.3), and N, U_g, U_c, and H are the four parameters that are varied to determine the local velocity profiles in this study. Typical examples of the profiles are shown in Fig. 2. Note that, as N increases, the thickness of each shear layer becomes thinner and hence the wake profile becomes closer to the so-called 'top-hat' profile. Also note that the ground distance H is varied in a certain range in this study such that the ground speed $U(-H)$ obtained from Eqs. (1)–(4) satisfies $U(-H) \geqslant 0.99U_g$ for a meaningful comparison with the earlier experiments using a moving ground [9].

It should be noted that the near wake profiles obtained from the above model are simplified or ideal ones; the real near wake profile of a bluff body depends on its cross-sectional geometry. The scope of the interest of this study is therefore limited to a qualitative description of the stability characteristics obtained. This, nonetheless, gives a possible explanation for the cessation of the Kármán vortex shedding in ground effect.

3. Analysis procedure

The absolute and convective instabilities of the above wake profiles are investigated in this study by using a local linear stability analysis, basically following Monkewitz and Nguyen [11]. The flow analysed is assumed to be quasi-laminar, i.e., the turbulence is assumed to affect the instability waves only indirectly through the mean velocity profile, not directly through its stresses. It is further assumed that the fluid is inviscid, as the instabilities of interest here are those of inviscid or inflectional type, and also that the flow is incompressible. It follows that the governing equations for the motion of small disturbances to be examined in this study can be derived from the Euler equations and the continuity equation as

$$\left(\frac{\partial}{\partial t}+U\frac{\partial}{\partial x}\right)u'+\frac{\mathrm{d}U}{\mathrm{d}y}v'+\frac{\partial p'}{\partial x}=0, \tag{5}$$

$$\left(\frac{\partial}{\partial t}+U\frac{\partial}{\partial x}\right)v'+\frac{\partial p'}{\partial y}=0, \tag{6}$$

$$\frac{\partial u'}{\partial x}+\frac{\partial v'}{\partial y}=0, \tag{7}$$

where u' and v' are the perturbation velocities in the x (streamwise) and y (transverse) directions, respectively, and p' is the perturbation pressure. $U(y)$ is the mean streamwise velocity obtained from the near wake model of Eqs. (1)–(4).

The above perturbation equations can be re-written with the perturbation stream function ψ' (by which the perturbation velocities are given as $u'=\partial\psi'/\partial y$ and $v'=-\partial\psi'/\partial x$) as

$$\left(\frac{\partial}{\partial t}+U\frac{\partial}{\partial x}\right)\nabla^2\psi'-\frac{\mathrm{d}^2U}{\mathrm{d}y^2}\frac{\partial\psi'}{\partial x}=0, \tag{8}$$

where $\nabla^2=(\partial^2/\partial x^2+\partial^2/\partial y^2)$. Since the main concern here is to show general criteria for the absolute and convective instabilities of the flow, the so-called normal-mode analysis is employed in this study, i.e., ψ' is expressed in the form of complex normal modes as

$$\psi'(x,y,t)=\phi(y)\exp\bigl[\mathrm{i}k(x-ct)\bigr], \tag{9}$$

where $k=k_r+\mathrm{i}k_i$ and $c=c_r+\mathrm{i}c_i$ denote the complex wave number and wave velocity, respectively. The complex frequency, $\omega=\omega_r+\mathrm{i}\omega_i$, is given by $\omega=kc=(k_rc_r-k_ic_i)+\mathrm{i}(k_rc_i+k_ic_r)$. Note that ω_i physically means the exponential growth rate of the disturbance wave in time. Substituting Eq. (9) into Eq. (8) finally leads to the well-known Rayleigh equation (see, e.g., Drazin and Reid [13]):

$$(U-c)\left(\frac{\mathrm{d}^2\phi}{\mathrm{d}y^2}-k^2\phi\right)-\frac{\mathrm{d}^2U}{\mathrm{d}y^2}\phi=0, \tag{10}$$

which, together with the boundary conditions

$$\phi=0 \quad \text{at } y=-H \text{ and } +\infty, \tag{11}$$

defines the stability eigenvalue problem to be numerically solved in this study [the dispersion relation is described as $\mathcal{F}(k,c)=0$, or alternatively $\mathcal{F}(k,\omega)=0$, and the corresponding nontrivial solution $\phi(y)$ is the eigenfunction].

The determination of whether the local velocity profile $U(y)$ is absolutely unstable or convectively unstable can be made by examining the branch-point singularities of the dispersion relation for k and ω based on the Briggs [14] – Bers [15] criterion. Specifically, the flow is found to be absolutely unstable (i.e., there exist unstable modes travelling upstream) if at least one of the branch-point singularities that satisfy the so-called pinching requirement is in the upper half of the complex ω plane (i.e., $\omega_i^0>0$, where the superscript 0 indicates the zero group velocity; see, e.g., Huerre [2] for a further description). This can be confirmed by mapping the dispersion relation $\omega(k)$ for constant k_r and k_i on the complex ω plane, or equivalently $k(\omega)$ for constant ω_r and ω_i on the complex k plane, as will be shown later in Section 4.

As concerns numerical methods employed in this study, the standard fourth-order Runge–Kutta method was used to numerically integrate Eq. (10), and then Muller's iterative method [16] was used to find complex eigenvalues satisfying the boundary conditions of Eq. (11). The whole procedure was repeated a number of times in order to map the dispersion relation $k(\omega)$ for each set of parameters (N, U_g, U_c, and H) and thereby to obtain the boundaries between the absolute and convective instabilities. All computations were performed using MATLAB [17].

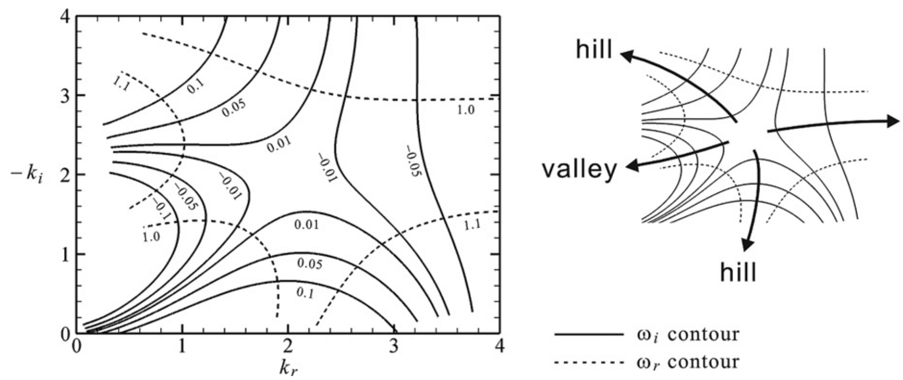

Fig. 3. Dispersion relation for an unbounded wake profile (sinuous mode, $N = 1$, $U_g/U_\infty = 1$, $U_c/U_\infty = 0.051$, $H/B = \infty$).

4. Results and discussion

4.1. Local instability characteristics of unbounded wakes

In order to validate the analysis procedure, first the analysis was applied to the unbounded wake profiles (i.e., $U_g/U_\infty = 1$ and $H/B = \infty$), which were originally investigated by Monkewitz and Nguyen [11]. For these symmetric wake profiles, two types of modes exist, namely the sinuous (or Kármán) and varicose modes, where the eigenfunction $\phi(y)$ takes the forms of even and odd functions about the origin $y = 0$, respectively. It is known that only the sinuous mode shows a sign of absolute instability for a physically realistic range of the parameters (N and U_c).

Fig. 3 shows the dispersion relation $k(\omega)$ for the sinuous mode for the wake profile described by Eqs. (1)–(4) with $N = 1$, $U_g/U_\infty = 1$, $U_c/U_\infty = 0.051$, and $H/B = \infty$. Note that the profile with the condition $N = 1$ corresponds to a fully-developed wake profile, and the spatial stability of this profile was first investigated by Betchov and Criminale [18]. It can be seen from this figure that, for this particular wake profile, the branch point singularity exists at $\omega_i \approx 0$ (and this branch point satisfies the pinching requirement, i.e., one of the two 'hills' consists of k^+ branches and the other consists of k^- branches in the terminology of Ref. [2]). Further analysis reveals that this branch point singularity is found at $\omega_i > 0$ when $U_c/U_\infty < 0.051$ and at $\omega_i < 0$ when $U_c/U_\infty > 0.051$, which means that $U_c = 0.051U_\infty$ is the critical centreline velocity of the wake, i.e., the flow is locally absolutely unstable when $U_c/U_\infty < 0.051$ and is locally convectively unstable when $U_c/U_\infty > 0.051$. This agrees with the results by Monkewitz and Nguyen [11] and also by Betchov and Criminale [18].

The analysis was also performed on the symmetric wake profiles with $N = 2$, 4, 12.5, and 25, and the critical U_c/U_∞ were found to be 0.089, 0.073, 0, and −0.032, respectively, which also agree with the results by Monkewitz and Nguyen [11]. Note that the wake becomes more unstable as N increases from 1 to about 2.3 but it becomes less unstable as N further increases [11].

4.2. Local instability characteristics of wakes in ground effect

In the following, the analysis is applied to the wake profiles in ground effect (i.e., U_g and H are now variables as well as N and U_c). Although the wake profiles are no longer symmetric, there still exist two types of modes in this case as the profile still possesses two inflection points: one of them (hereafter referred to as Mode I) shows the eigenfunction $\phi(y)$ taking the form of even functions and the other (hereafter referred to as Mode II) shows that of odd functions when H/B is sufficiently large. Since Mode II showed no signs of absolute instability for a physically realistic range of the parameters, only the results for Mode I are shown and discussed below.

Fig. 4 shows an example of the influence of the relative ground distance H/B on the branch points of the dispersion relation (for the profiles with $N = 12.5$, $U_g/U_\infty = 1$, and $U_c/U_\infty = 0$). Here the curves labelled 'Mode I-A' indicate the mode corresponding to the sinuous mode for the unbounded wake when H/B is sufficiently large. This can be confirmed from $\omega_i^0 \to 0$ as $H/B \to \infty$, which is consistent with the result by Monkewitz and Nguyen [11] noted in Section 4.1 that $U_c = 0$ is the critical centreline velocity for the unbounded wake profile with $N = 12.5$. As H/B decreases to less than about 1.6, however, another branch point with a larger ω_i^0 value (labelled 'Mode I-B' in the

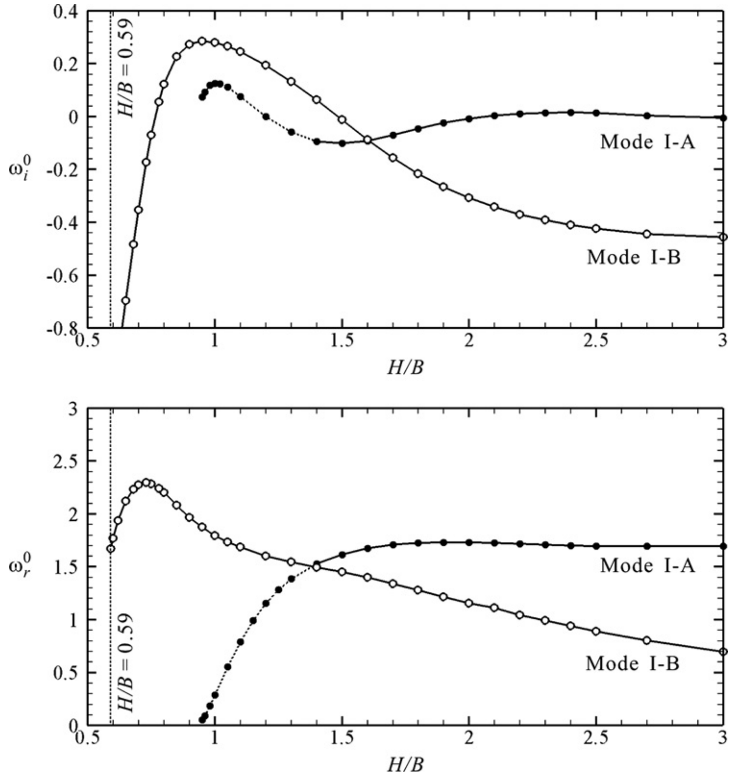

Fig. 4. Influence of H/B on the imaginary and real parts of ω at the branch points ($N = 12.5$, $U_g/U_\infty = 1$, $U_c/U_\infty = 0$).

figure) appears on the dispersion relation. The key question here is whether this second branch point is relevant to the stability of the wake, or in other words, whether this branch point arises from the coalescence of upstream-propagating k^+ branches and downstream-propagating k^- branches.

Fig. 5 shows the maps of the dispersion relation for the cases with $H/B = 1.7$, 1.5, and 1.3. At $H/B = 1.7$ [Fig. 5(a)], both branch points are of the so-called k^+/k^- type, which can be verified from the fact that, for each branch point, one of the two hills originates in the $k_i > 0$ region and the other originates in the $k_i < 0$ region. Mode I-A still has a larger ω_i^0 value than Mode I-B [cf. Fig. 4], and hence has a dominant influence on the stability characteristics of the wake. At $H/B = 1.5$ [Fig. 5(b)], again both branch points are of the k^+/k^- type, but the ω_i^0 value of Mode I-A is now smaller than that of Mode I-B [cf. Fig. 4]. This means that the more unstable mode is shifted from Mode I-A to Mode I-B as H/B is reduced from 1.7 to 1.5. Of interest is that, at $H/B = 1.3$ [Fig. 5(c)], the branch point for Mode I-A is no longer of the k^+/k^- type but of the k^-/k^- type, i.e., Mode I-A is not relevant to the stability characteristics of the wake when $H/B \leqslant 1.3$.

The value of ω_i^0 for Mode I-B becomes larger than zero as H/B decreases to less than 1.5 (cf. Fig. 4), which physically means that the wake becomes absolutely unstable in this H/B range. As H/B further decreases to less than about 0.95, however, ω_i^0 for Mode I-B rapidly decreases, and finally the state of the wake changes back to being convectively unstable for $H/B < 0.77$. It should be noted that the analysis for this example was performed for $H/B \geqslant 0.59$, in which range the condition of $U(-H) \geqslant 0.99U_\infty$ is maintained for the wake profile with $N = 12.5$, and ω_i^0 at $H/B = 0.59$ was found to be -1.09. This suggests a strong 'stabilising' effect of the nearby ground on the wake.

The main focus of the discussion is now on the transition between the absolute and convective instabilities especially in the smaller H/B region, which was observed around $H/B = 0.77$ in the above example with $N = 12.5$, $U_g/U_\infty = 1$, and $U_c/U_\infty = 0$. Figs. 6(a) and 6(b) show the absolute instability boundaries in the (U_c/U_∞)–(H/B) plane for different N and for different U_g/U_∞, respectively. Note that the kink of each curve around $H/B = 1.5$ corresponds to the turnover of the more unstable mode between Mode I-A and Mode I-B described in the above example in Figs. 4 and 5. Also note that the range $N \geqslant 4$ shown here corresponds to the 'top-hat-like'

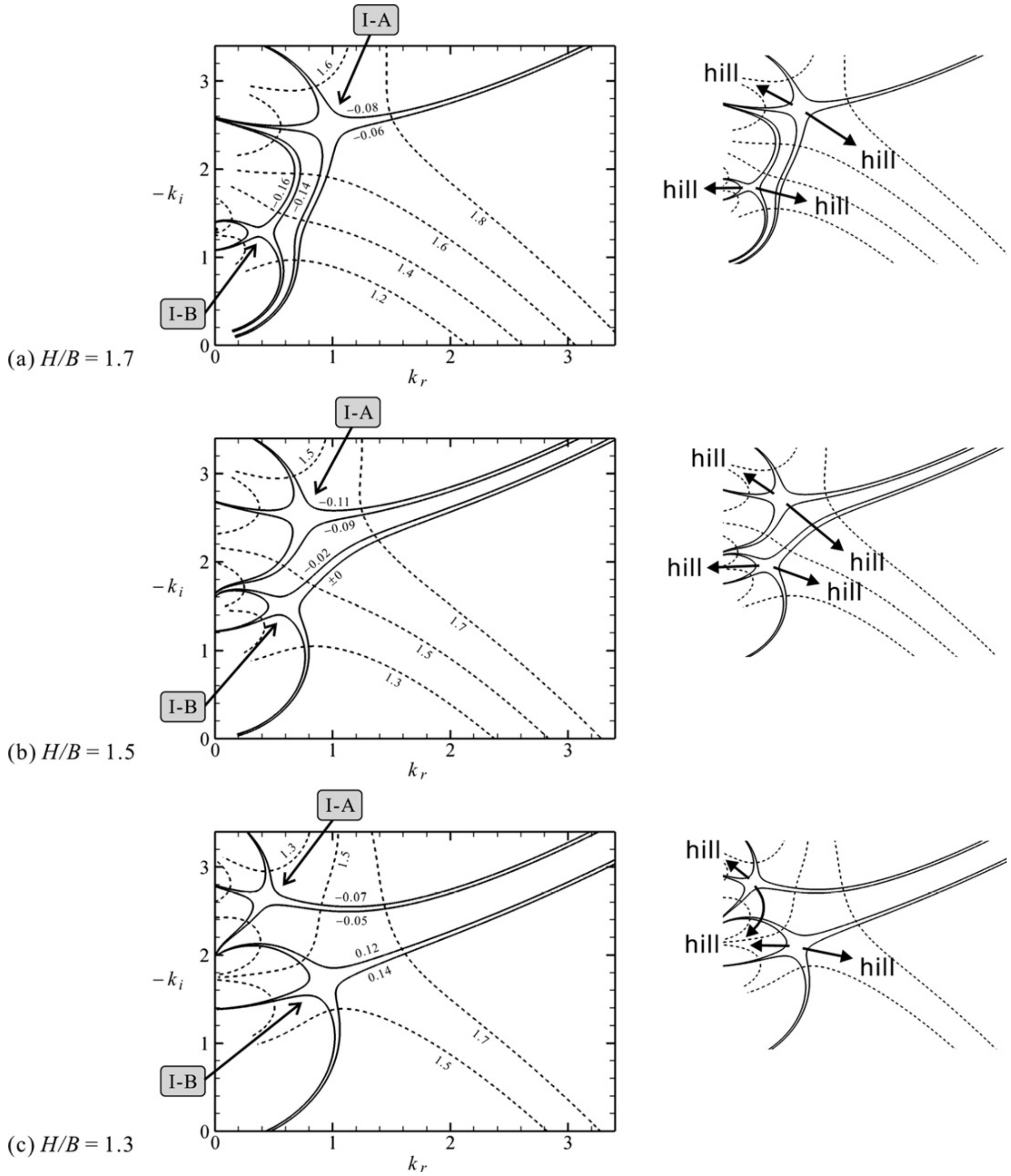

Fig. 5. Dispersion relation for local wake profiles ($N = 12.5$, $U_g/U_\infty = 1$, $U_c/U_\infty = 0$) with three different H/B; solid and dashed lines indicate the contours of ω_i and ω_r, respectively.

near-wake profiles that are of interest in this study (cf. Fig. 2), whereas the range $0.8 \leqslant U_g/U_\infty \leqslant 1.2$ covers almost completely the corresponding (hypothetical) velocity-ratio range experimentally observed in the near wake region of a circular cylinder in Ref. [9], as shown later in Fig. 9(c). For all the cases shown in Fig. 6, it can be seen that the critical centreline velocity rapidly decreases as H/B decreases to less than about 0.9. This again shows the strong stabilising effect of the nearby ground on the wake; at $H/B = 0.6$, for example, the wake with $N = 12.5$, $U_g/U_\infty = 1$, and $U_c/U_\infty = -0.4$ is still within the region of convectively unstable rather than absolutely unstable, despite its strong backflow.

Of further interest is the influence of the wake parameters N and U_g/U_∞ on the results. As concerns the influence of N, it can be seen from Fig. 6(a) that the profiles with smaller N (i.e., with thicker mixing layers, cf. Fig. 2) are more

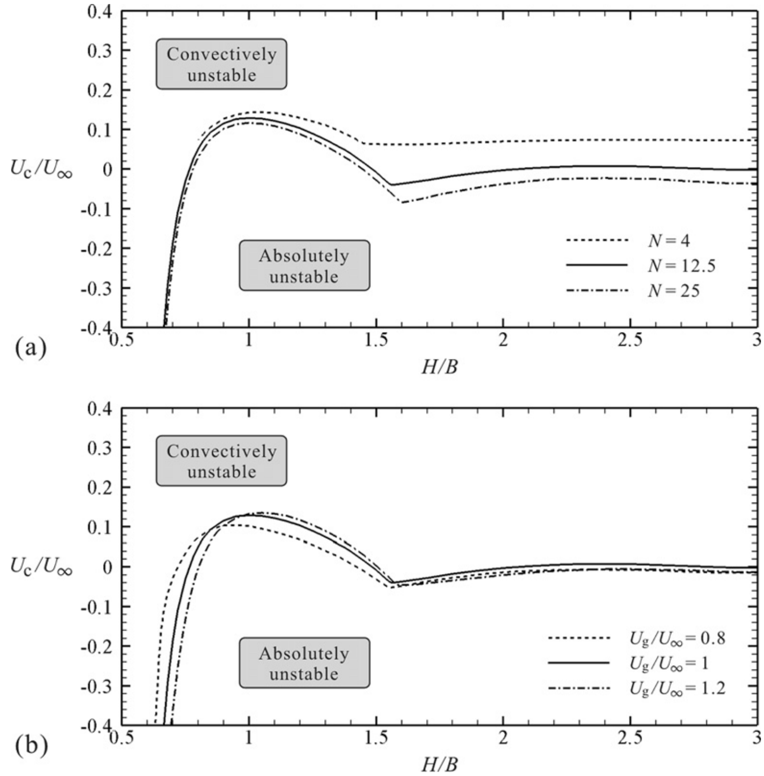

Fig. 6. Absolute instability boundaries in the (U_c/U_∞)–(H/B) plane: (a) for different N with $U_g/U_\infty = 1$; (b) for different U_g/U_∞ with $N = 12.5$.

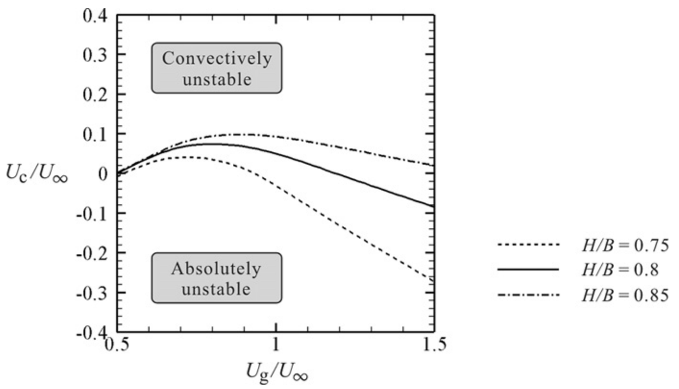

Fig. 7. Absolute instability boundaries in the (U_c/U_∞)–(U_g/U_∞) plane for different H/B (with $N = 12.5$).

absolutely unstable than the profiles with larger N (i.e., with thinner mixing layers) for the range of $N \geqslant 4$ examined here. This tendency has already been reported by Monkewitz and Nguyen [11] for the unbounded wake profiles with $U_g/U_\infty = 1$ and $H/B = \infty$, as noted in Section 4.1. For $H/B \leqslant 0.9$, however, there seems to be little influence of N on the stability characteristics of the wake, although the analysis for $N = 4$ was performed only for $H/B \geqslant 0.8$ so as to maintain the condition of $U(-H) \geqslant 0.99U_\infty$ in this study.

As for the influence of U_g/U_∞, only small differences can be seen in the results [Fig. 6(b)] in the larger H/B regime. For $H/B \leqslant 0.85$, however, the figure shows an interesting trend that the wake becomes more absolutely unstable as U_g/U_∞ decreases. Fig. 7 shows the absolute instability boundaries in the (U_c/U_∞)–(U_g/U_∞) plane for $H/B = 0.75$, 0.8, and 0.85. It can be seen that the most unstable U_g/U_∞ range shifts towards $U_g/U_\infty < 1$ as H/B decreases. That is to say, the wake becomes more unstable as the velocity on the 'near-ground' side is slightly decreased compared with that on the 'far-ground' side. This interesting influence of U_g/U_∞ on the local linear stability characteristics of the wake might be related to the counter-intuitive experimental observation by Lei et al. [7] that the critical gap ratio for the onset/cessation of the Kármán vortex shedding decreased as the boundary layer thickness on the ground *increased*, as discussed later in the next section.

4.3. Global instability and the cessation of Kármán vortex shedding in ground effect

In the previous section, the linear stability characteristics of local wake profiles in ground effect were investigated. In summary the results showed that, when the relative ground distance H/B is small, the local linear stability characteristics of the wake are largely affected by the parameters H/B, U_c/U_∞, and U_g/U_∞, but not by N. In this section, further investigations are performed to discuss the link between the local linear stability characteristics and the cessation of the Kármán vortex shedding in ground effect. Specifically, the local linear stability analysis performed in the previous section is now applied to velocity profiles varying in the streamwise direction so as to examine the streamwise variation of the local stability characteristics of the wake in ground effect.

This type of analysis has been successful for many types of spatially developing flows [19–23] since several researchers suggested in the mid-1980s a close link between the local linear stability characteristics and the global mode selection of the flows [24,25,11]. Among them, Monkewitz and Nguyen [11] proposed the 'initial resonance criterion' for the wakes of two-dimensional bluff bodies; that is, the global mode (i.e., the overall frequency and associated spatial structures) of the wake is determined by the local resonance at the first streamwise station of local absolute instability. This scenario was recently found to be the case not only in the framework of linear stability theory but also in the theory of 'steep nonlinear global modes', which was first identified in a model problem using the one-dimensional complex Ginzburg–Landau equation by Pier et al. [26] and was then confirmed in the context of real wake flows governed by the Navier–Stokes equations by Pier and Huerre [12]. According to these authors, the upstream edge or 'front' of the region of local linear absolute instability acts as a wavemaker to generate nonlinear waves travelling downstream and imposes its local frequency on the global oscillation of the downstream flow. Hence the results of the linear stability analysis presented here would give some useful insights into the physics of the cessation of the real (nonlinear) Kármán vortex shedding in ground effect.

In this study, the streamwise variation of the wake profile is determined based on the results of the earlier experiments by the authors [9] on a circular cylinder placed near a moving ground (at an upper-subcritical Reynolds number of 4.0×10^4 based on the cylinder diameter d). Specifically, the local wake parameters corresponding to H/B, U_c/U_∞, and U_g/U_∞ are extracted from the experimental mean velocity profiles at several streamwise positions behind the cylinder. The influence of the parameter N is assumed to be negligible, according to the results in the previous section (note that only the small gap range of $H/B < 0.9$ is of interest in this section). An example of the comparison between the experimental data [9] and the model wake profile is shown in Fig. 8. Since the real (experimental) near wake profiles have velocity overshoots on both sides of the wake, here the parameters U_∞ and U_g for the

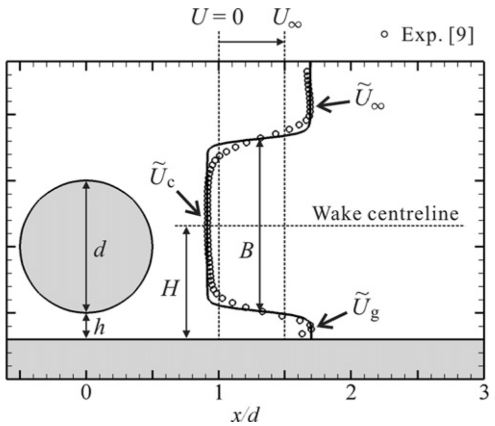

Fig. 8. Example of a comparison of local wake profiles; open circles show the experimental results [9] ($h/d = 0.2$, $x/d = 1$) and the solid line shows the model profile ($\tilde{U}_\infty = 1.381U_\infty$, $\tilde{U}_g = 1.400U_\infty$, $\tilde{U}_c = -0.172U_\infty$, $H = 0.866d$, $B = 1.299d$, $N = 12.5$).

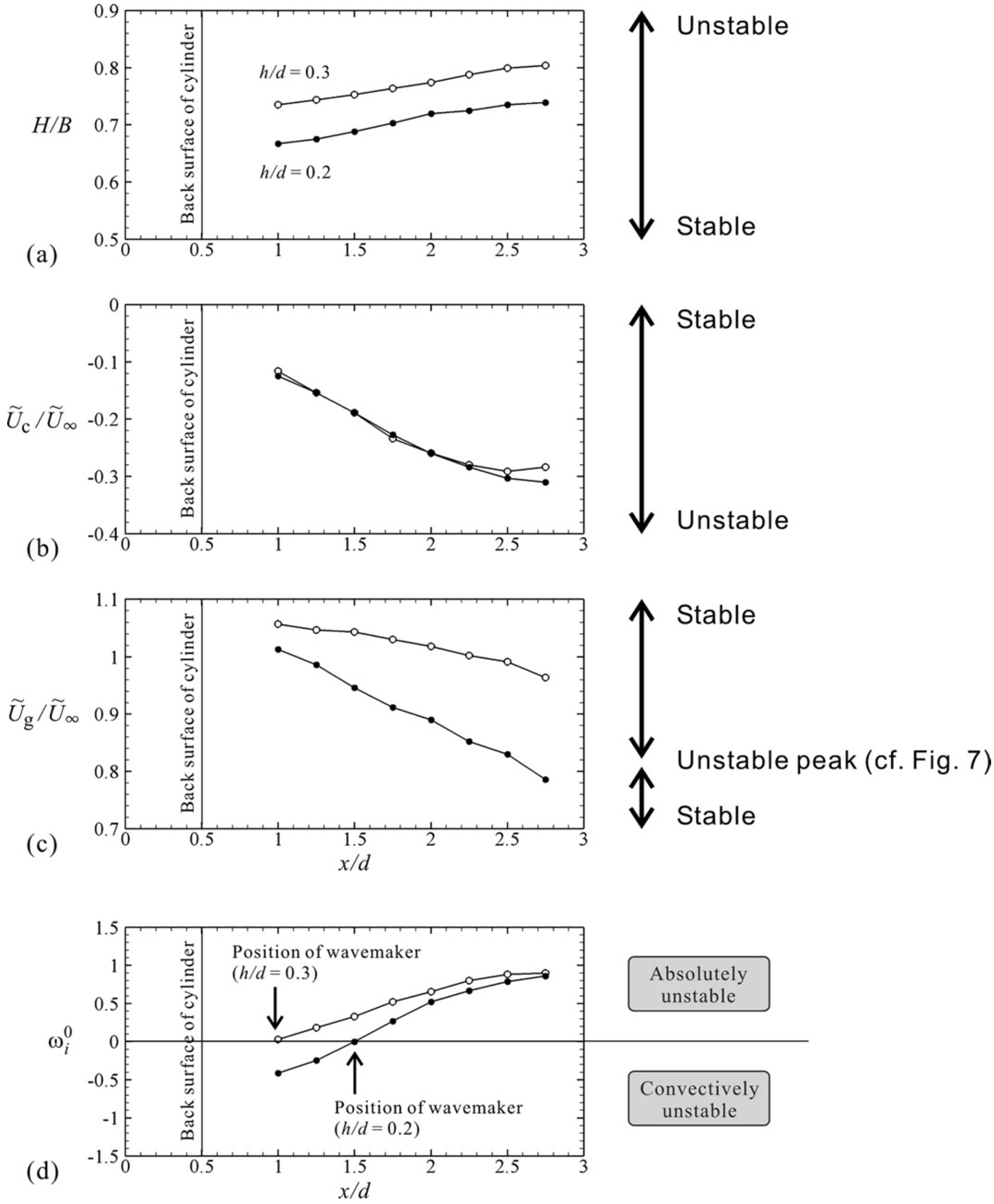

Fig. 9. Streamwise variation of the local stability characteristics of circular cylinder wakes in ground effect: (a)–(c) local wake parameters extracted from the experimental data [9], and (d) local stability characteristics calculated based on the extracted parameters.

model wake profiles are determined by the two local maximum velocities on each side of the wake (hereafter referred to as $\tilde{U}_\infty$ and $\tilde{U}_g$), respectively. The parameter U_c, meanwhile, is determined by the minimum velocity of the wake (hereafter referred to as $\tilde{U}_c$) rather than by the centreline velocity of the wake. The wake width B is determined by the transverse distance between the two points where the streamwise velocity reaches $(\tilde{U}_c + \tilde{U}_\infty)/2$ and $(\tilde{U}_c + \tilde{U}_g)/2$, respectively. The ground distance H is determined by the distance from the ground surface to the centreline of the two transverse positions that define the wake width B. In addition to these extracted parameters, a constant N of 12.5 is retained for the following analysis.

Figs. 9(a)–(c) show the streamwise variation of the local wake parameters H/B, $\tilde{U}_c/\tilde{U}_\infty$, and $\tilde{U}_g/\tilde{U}_\infty$ extracted from the experimental mean velocity profiles behind the cylinder at two different gap ratios h/d of 0.2 and 0.3. Note that, in the experiments, the Kármán vortex shedding was found to be suppressed (at least in the near wake region of $x/d \leqslant 2.75$) at these two gap ratios [9]. Also note that the figures show the variation of the wake parameters at $1 \leqslant x/d \leqslant 2.75$, in which region the experimental local velocity profiles showed common characteristics (i.e., having a local maximum on each side of the wake and also a local minimum near the centreline of the wake) and were therefore able to be approximated by the model wake profiles in the manner described above. It can be seen from the figures that, for both h/d cases, H/B gradually increases in the downstream direction since the flow is slightly deflected upward in this region [9]. It is also obvious that, at each streamwise position, H/B decreases as h/d decreases. Meanwhile, $\tilde{U}_c/\tilde{U}_\infty$ becomes increasingly negative in the downstream direction since this region corresponds to the upstream part of the large recirculation region behind the cylinder [9]. However, the difference in the variation of $\tilde{U}_c/\tilde{U}_\infty$ between the two h/d cases appears to be very small. The velocity ratio $\tilde{U}_g/\tilde{U}_\infty$ also decreases as the wake develops downstream. This is because, on the far-ground side of the wake the ambient fluid is entrained (i.e., momentum is supplied) as the shear layer spreads, whereas on the near-ground side of the wake no supply of the ambient fluid is available and thus the velocity overshoot diminishes faster than that on the far-ground side. This also explains the reason why $\tilde{U}_g/\tilde{U}_\infty$ decreases faster at $h/d = 0.2$ than at $h/d = 0.3$.

Fig. 9(d) shows the streamwise variation of ω_i^0 calculated based on the extracted local wake parameters shown in Figs. 9(a)–(c). Note that $\omega_i^0 > 0$ physically means that the wake is locally absolutely unstable, as discussed in the previous section. It can be seen that the state of the (very) near wake region changes from being absolutely unstable to being convectively unstable as the gap ratio h/d decreases. This local stabilisation in the (very) near wake region is mainly explained by the decrease in the relative gap distance H/B shown in Fig. 9(a). In the region further downstream, however, there still exists an absolutely unstable region, the front of which is located around $x/d = 1$ for $h/d = 0.3$, and at $x/d = 1.5$ for $h/d = 0.2$. This is largely due to the strong backflow in this region, as shown in Fig. 9(b). According to Pier and Huerre [12], this front should act as a wavemaker to generate nonlinear travelling waves and a self-sustained global oscillation should develop downstream of the front — this is not quantitatively consistent with the experimental observation [9] that the Kármán vortex shedding was suppressed at these gap ratios, at least in the region of $x/d \leqslant 2.75$. In addition, the local frequency ω_r^0 at the front of the locally absolutely unstable region was found in the stability analysis to be 2.52 (for $h/d = 0.3$) and 2.31 (for $h/d = 0.2$), which correspond to the Strouhal number (based on the cylinder diameter d rather than on the local wake width B) of 0.31 and 0.27, respectively. Although the corresponding experimental data (for a cylinder near a moving ground) were not measured in Ref. [9], Bearman and Zdravkovich [6] have reported (for a cylinder near a fixed ground) that the frequency of the Kármán vortex shedding in the near wake region was almost constant at about 0.21 for $h/d \geqslant 0.3$ — again some quantitative differences exist between the experiments and the stability analysis.

These quantitative differences might be explained by the fact that the experiments [9,6] were carried out in the upper-subcritical Reynolds number regime, i.e., the near wake of the cylinder was fully turbulent regardless of whether or not the Kármán-type vortex shedding was suppressed by the ground effect. In the stability analysis, on the other hand, the flow was assumed to be quasi-laminar, i.e., the turbulence was assumed to affect the (organised) instability waves only indirectly through the mean velocity profile. This assumption, however, generally leads to only qualitatively correct results when applied to fully turbulent shear flows [27]. Another possible cause of the differences might be the simple representation of the velocity profile near the ground used in the stability analysis. It should be noted that, in the experiments [9], even though the ground was moving at the same speed as the free stream, a very thin boundary layer still existed on the moving ground (due to the local acceleration of the flow between the cylinder and the ground). Although the scale of this thin boundary layer is much smaller than that of the wake, its influence on the stability characteristics of the wake is still unclear. Nevertheless, it may be concluded that the present stability analysis has qualitatively indicated some fundamental mechanisms of the cessation of the Kármán vortex shedding in the near wake region of the cylinder in ground effect.

Some additional comments are made below on the influence of the velocity ratio $\tilde{U}_g/\tilde{U}_\infty$ on the onset and cessation of the Kármán vortex shedding in ground effect. It was shown in Section 4.2 that the local model wake profile becomes more absolutely unstable as the velocity on the near-ground side (U_g) is slightly decreased compared with that on the far-ground side (U_∞) when the relative gap distance H/B is small [cf. Fig. 7]. Here, if we (boldly) assume that the near wake profile behind a cylinder placed near a fixed ground (on which a boundary layer of a certain thickness exists) may also be approximated by the model wake profile used in this study, the trend of the influence of U_g/U_∞ (and thus of $\tilde{U}_g/\tilde{U}_\infty$) qualitatively agrees with the counter-intuitive experimental observation by Lei et al. [7] that the critical gap ratio for the onset/cessation of the Kármán vortex shedding decreased as the boundary layer thickness on the ground *increased*. This might be explained from the viewpoint of the stability of the wake because the flow through the gap between the cylinder and the ground decreases (which might be considered to correspond to a slight decrease in $\tilde{U}_g/\tilde{U}_\infty$ and to make the wake more unstable) when the boundary layer thickness increases. In other words, as the boundary layer thickness on the ground increases the so-called 'effective' gap ratio might be considered to decrease, but in a way such that $\tilde{U}_g/\tilde{U}_\infty$ decreases [like that described in Fig. 9(c)] and not such that H/B decreases [like that described in Fig. 9(a)].

5. Conclusions

Local and global stability characteristics of the wakes of general two-dimensional bluff bodies placed near and parallel to a ground were investigated by using a linear normal-mode stability analysis. The analysis was first applied to the four-parameter (i.e., N, U_c/U_∞, U_g/U_∞, and H/B) family of local velocity profiles, which was proposed in this study as an extended version of the two-parameter symmetric near wake model by Monkewitz and Nguyen [11] and Monkewitz [3], to investigate the fundamental local linear stability characteristics of the wakes in ground effect. For $H/B \leqslant 0.9$ (roughly corresponding to $h/d < 0.4$, in which range the onset/cessation of the Kármán vortex shedding takes place for the case of a circular cylinder), the local wake profiles were found to become more unstable when the relative centreline velocity (U_c/U_∞) decreases, and also when the relative ground distance (H/B) increases. In addition, the wake was found to become more unstable when the velocity on the near-ground side (U_g) is slightly smaller than that on the far-ground side (U_∞) [cf. Fig. 7]. The influence of the shape factor (N) of the wake, however, was found to be very small in this H/B range.

The local linear analysis was then compared with the experiments on a circular cylinder placed near a moving ground [9] to discuss the global instability of the wake in ground effect. Specifically, the local linear analysis was applied to the model wake profiles with the parameters corresponding to H/B, U_c/U_∞, and U_g/U_∞ extracted from the experimental mean velocity data at several streamwise positions behind the cylinder. The streamwise variation of the local linear stability characteristics of the wake was then examined based on the transition scenario of 'steep global modes' by Pier and Huerre [12]. The results indicated that the very near wake of the cylinder changes from being absolutely unstable to being convectively unstable when the cylinder comes close to the ground. This seems qualitatively consistent with the transition scenario of the global mode for general wake-type flows, i.e., the cessation of the Kármán vortex shedding in the near wake region of the cylinder in ground effect may also be explained by the change of the near wake from being absolutely unstable to being convectively unstable, in analogy with the case for a cylinder equipped with a backward splitter plate [5]. The quantitative agreement between the experiments and the stability analysis, however, was not good: the upstream edge of the absolutely unstable region was found in the stability analysis to be around $x/d = 1$ when $h/d = 0.3$ and $x/d = 1.5$ when $h/d = 0.2$, whereas in the experiments [9] the Kármán vortex shedding was found to be suppressed at least in the region of $x/d \leqslant 2.75$ at these gap ratios.

Discussions were also given to the cessation of the Kármán vortex shedding from a cylinder placed near a fixed ground, for which Lei et al. [7] experimentally observed that the critical gap ratio for the onset/cessation of the Kármán vortex shedding decreased as the boundary layer thickness on the ground *increased*. Although direct comparison between the analysis and the experiments was not possible for this fixed ground case, the observation by Lei et al. [7] might also be explained by the results of the stability analysis in this study. That is, the wake might be considered to become more unstable when the boundary layer thickness increases because the flow through the gap between the cylinder and the ground decreases, presumably corresponding to a slight decrease in the velocity ratio $\tilde{U}_g/\tilde{U}_\infty$. In other words, the decrease in the critical gap ratio due to the increase in the boundary layer thickness on the ground might be explained by the decrease in the so-called 'effective' gap ratio, but in a way such that the velocity ratio $\tilde{U}_g/\tilde{U}_\infty$ decreases to make the wake more unstable, and not such that the relative ground distance H/B decreases to make the wake more stable.

Acknowledgement

T. Nishino is supported by a research scholarship from the School of Engineering Sciences, University of Southampton, United Kingdom. The authors wish to thank Professor Neil D. Sandham for many useful discussions.

References

[1] P. Huerre, P.A. Monkewitz, Local and global instabilities in spatially developing flows, Annu. Rev. Fluid Mech. 22 (1990) 473–537.
[2] P. Huerre, Open shear flow instabilities, in: G.K. Batchelor, H.K. Moffat, M.G. Worster (Eds.), Perspectives in Fluid Dynamics: A Collective Introduction to Current Research, Cambridge University Press, Cambridge, UK, 2000, pp. 159–229.
[3] P.A. Monkewitz, The absolute and convective nature of instability in two-dimensional wakes at low Reynolds numbers, Phys. Fluids 31 (1988) 999–1006.
[4] A. Roshko, On the wake and drag of bluff bodies, J. Aeronaut. Sci. 22 (1955) 124–132.
[5] H. Oertel Jr., Wakes behind blunt bodies, Annu. Rev. Fluid Mech. 22 (1990) 539–564.
[6] P.W. Bearman, M.M. Zdravkovich, Flow around a circular cylinder near a plane boundary, J. Fluid Mech. 89 (1978) 33–47.
[7] C. Lei, L. Cheng, K. Kavanagh, Re-examination of the effect of a plane boundary on force and vortex shedding of a circular cylinder, J. Wind Eng. Ind. Aerodyn. 80 (1999) 263–286.
[8] S.J. Price, D. Sumner, J.G. Smith, K. Leong, M.P. Paidoussis, Flow visualization around a circular cylinder near to a plane wall, J. Fluids Struct. 16 (2002) 175–191.
[9] T. Nishino, G.T. Roberts, X. Zhang, Vortex shedding from a circular cylinder near a moving ground, Phys. Fluids 19 (2007) 025103.
[10] C.H.K. Williamson, Vortex dynamics in the cylinder wake, Annu. Rev. Fluid Mech. 28 (1996) 477–539.
[11] P.A. Monkewitz, L.N. Nguyen, Absolute instability in the near-wake of two-dimensional bluff bodies, J. Fluids Struct. 1 (1987) 165–184.
[12] B. Pier, P. Huerre, Nonlinear self-sustained structures and fronts in spatially developing wake flows, J. Fluid Mech. 435 (2001) 145–174.
[13] P.G. Drazin, W.H. Reid, Hydrodynamic Stability, Cambridge University Press, Cambridge, UK, 1981.
[14] R. Briggs, Electron-Stream Interaction with Plasmas, MIT Press, MA, USA, 1964.
[15] A. Bers, Space-time evolution of plasma instabilities — absolute and convective, in: M.N. Rosenbluth, R.Z. Sagdeev (Eds.), Handbook of Plasma Physics, North-Holland, Amsterdam, 1983, pp. 451–517.
[16] W.H. Press, S.A. Teukolsky, W.T. Vetterling, B.P. Flannery, Numerical Recipes in FORTRAN, second ed., Cambridge University Press, Cambridge, UK, 1992, p. 364.
[17] The MathWorks, Inc., Using MATLAB, The MathWorks, Inc., Natick, MA, USA, 2002.
[18] R. Betchov, W.O. Criminale, Spatial instability of the inviscid jet and wake, Phys. Fluids 9 (1966) 359–362.
[19] D. Chen, G.H. Jirka, Absolute and convective instabilities of plane turbulent wakes in a shallow water layer, J. Fluid Mech. 338 (1997) 157–172.
[20] D.A. Hammond, L.G. Redekopp, Global dynamics of symmetric and asymmetric wakes, J. Fluid Mech. 331 (1997) 231–260.
[21] D.A. Hammond, L.G. Redekopp, Local and global instability properties of separation bubbles, Eur. J. Mech. B Fluids 17 (1998) 145–164.
[22] M. Alam, N.D. Sandham, Direct numerical simulation of 'short' laminar separation bubbles with turbulent reattachment, J. Fluid Mech. 410 (2000) 1–28.
[23] I.P. Castro, The stability of laminar symmetric separated wakes, J. Fluid Mech. 532 (2005) 389–411.
[24] R.T. Pierrehumbert, Local and global baroclinic instability of zonally varying flow, J. Atmos. Sci. 41 (1984) 2141–2162.
[25] W. Koch, Local instability characteristics and frequency determination of self-excited wake flows, J. Sound Vib. 99 (1985) 53–83.
[26] B. Pier, P. Huerre, J.-M. Chomaz, A. Couairon, Steep nonlinear global modes in spatially developing media, Phys. Fluids 10 (1998) 2433–2435.
[27] W.C. Reynolds, A.K.M.F. Hussain, The mechanics of an organized wave in turbulent shear flow. Part 3. Theoretical models and comparisons with experiments, J. Fluid Mech. 54 (1972) 263–288.